

Rare B Decays to States Containing a J/ψ Meson

The *BABAR* Collaboration

November 13, 2018

Abstract

We report preliminary measurements of the branching fractions for $B^+ \rightarrow J/\psi\phi K^+$, $B^0 \rightarrow J/\psi\phi K_S^0$, $B^0 \rightarrow J/\psi\phi$, $B^0 \rightarrow J/\psi\eta$ and $B^0 \rightarrow J/\psi\eta'$ using 56 million $B\bar{B}$ events collected at the $\Upsilon(4S)$ resonance with the *BABAR* detector at PEP-II. We measure branching fractions of $\mathcal{B}(B^+ \rightarrow J/\psi\phi K^+) = (4.4 \pm 1.4(stat) \pm 0.7(syst)) \times 10^{-5}$ and $\mathcal{B}(B^0 \rightarrow J/\psi\phi K_S^0) = (5.1 \pm 1.9(stat) \pm 0.9(syst)) \times 10^{-5}$, and set upper limits at 90% C.L. for branching fractions $\mathcal{B}(B^0 \rightarrow J/\psi\phi) < 0.95 \times 10^{-5}$, $\mathcal{B}(B^0 \rightarrow J/\psi\eta) < 2.7 \times 10^{-5}$, and $\mathcal{B}(B^0 \rightarrow J/\psi\eta') < 6.4 \times 10^{-5}$.

Presented at the XXXVIIth Rencontres de Moriond on QCD and Hadronic Interactions,
3-16—3/23/2002, Les Arcs, Savoie, France

Stanford Linear Accelerator Center, Stanford University, Stanford, CA 94309

Work supported in part by Department of Energy contract DE-AC03-76SF00515.

The *BABAR* Collaboration,

B. Aubert, D. Boutigny, J.-M. Gaillard, A. Hicheur, Y. Karyotakis, J. P. Lees, P. Robbe, V. Tisserand,
A. Zghiche

Laboratoire de Physique des Particules, F-74941 Annecy-le-Vieux, France

A. Palano, A. Pompili

Università di Bari, Dipartimento di Fisica and INFN, I-70126 Bari, Italy

G. P. Chen, J. C. Chen, N. D. Qi, G. Rong, P. Wang, Y. S. Zhu

Institute of High Energy Physics, Beijing 100039, China

G. Eigen, I. Ofte, B. Stugu

University of Bergen, Inst. of Physics, N-5007 Bergen, Norway

G. S. Abrams, A. W. Borgland, A. B. Breon, D. N. Brown, J. Button-Shafer, R. N. Cahn, E. Charles,
M. S. Gill, A. V. Gritsan, Y. Groysman, R. G. Jacobsen, R. W. Kadel, J. Kadyk, L. T. Kerth,
Yu. G. Kolomensky, J. F. Kral, C. LeClerc, M. E. Levi, G. Lynch, L. M. Mir, P. J. Oddone, M. Pripstein,
N. A. Roe, A. Romosan, M. T. Ronan, V. G. Shelkov, A. V. Telnov, W. A. Wenzel

Lawrence Berkeley National Laboratory and University of California, Berkeley, CA 94720, USA

T. J. Harrison, C. M. Hawkes, D. J. Knowles, S. W. O'Neale, R. C. Penny, A. T. Watson, N. K. Watson
University of Birmingham, Birmingham, B15 2TT, United Kingdom

T. Deppermann, K. Goetzen, H. Koch, B. Lewandowski, K. Peters, H. Schmuecker, M. Steinke
Ruhr Universität Bochum, Institut für Experimentalphysik 1, D-44780 Bochum, Germany

N. R. Barlow, W. Bhimji, N. Chevalier, P. J. Clark, W. N. Cottingham, B. Foster, C. Mackay, F. F. Wilson
University of Bristol, Bristol BS8 1TL, United Kingdom

K. Abe, C. Hearty, T. S. Mattison, J. A. McKenna, D. Thiessen
University of British Columbia, Vancouver, BC, Canada V6T 1Z1

S. Jolly, A. K. McKemey
Brunel University, Uxbridge, Middlesex UB8 3PH, United Kingdom

V. E. Blinov, A. D. Bukin, D. A. Bukin, A. R. Buzykaev, V. B. Golubev, V. N. Ivanchenko, A. A. Korol,
E. A. Kravchenko, A. P. Onuchin, S. I. Serednyakov, Yu. I. Skovpen, A. N. Yushkov
Budker Institute of Nuclear Physics, Novosibirsk 630090, Russia

D. Best, M. Chao, D. Kirkby, A. J. Lankford, M. Mandelkern, S. McMahon, D. P. Stoker
University of California at Irvine, Irvine, CA 92697, USA

K. Arisaka, C. Buchanan, S. Chun
University of California at Los Angeles, Los Angeles, CA 90024, USA

D. B. MacFarlane, S. Prell, Sh. Rahatlou, G. Raven, V. Sharma
University of California at San Diego, La Jolla, CA 92093, USA

C. Campagnari, B. Dahmes, P. A. Hart, N. Kuznetsova, S. L. Levy, O. Long, A. Lu, M. A. Mazur,
J. D. Richman, W. Verkerke

University of California at Santa Barbara, Santa Barbara, CA 93106, USA

J. Beringer, A. M. Eisner, M. Grothe, C. A. Heusch, W. S. Lockman, T. Pulliam, T. Schalk, R. E. Schmitz,
B. A. Schumm, A. Seiden, M. Turri, W. Walkowiak, D. C. Williams, M. G. Wilson

University of California at Santa Cruz, Institute for Particle Physics, Santa Cruz, CA 95064, USA

E. Chen, G. P. Dubois-Felsmann, A. Dvoretskii, D. G. Hitlin, S. Metzler, J. Oyang, F. C. Porter, A. Ryd,
A. Samuel, S. Yang, R. Y. Zhu

California Institute of Technology, Pasadena, CA 91125, USA

S. Jayatilleke, G. Mancinelli, B. T. Meadows, M. D. Sokoloff

University of Cincinnati, Cincinnati, OH 45221, USA

T. Barillari, P. Bloom, W. T. Ford, U. Nauenberg, A. Olivas, P. Rankin, J. Roy, J. G. Smith, W. C. van
Hoek, L. Zhang

University of Colorado, Boulder, CO 80309, USA

J. Blouw, J. L. Harton, M. Krishnamurthy, A. Soffer, W. H. Toki, R. J. Wilson, J. Zhang

Colorado State University, Fort Collins, CO 80523, USA

T. Brandt, J. Brose, T. Colberg, M. Dickopp, R. S. Dubitzky, A. Hauke, E. Maly, R. Müller-Pfefferkorn,
S. Otto, K. R. Schubert, R. Schwierz, B. Spaan, L. Wilden

Technische Universität Dresden, Institut für Kern- und Teilchenphysik, D-01062 Dresden, Germany

D. Bernard, G. R. Bonneauaud, F. Brochard, J. Cohen-Tanugi, S. Ferrag, S. T'Jampens, Ch. Thiebaux,
G. Vasileiadis, M. Verderi

Ecole Polytechnique, LLR, F-91128 Palaiseau, France

A. Anjomshoaa, R. Bernet, A. Khan, D. Lavin, F. Muheim, S. Playfer, J. E. Swain, J. Tinslay

University of Edinburgh, Edinburgh EH9 3JZ, United Kingdom

M. Falbo

Elon University, Elon College, NC 27244-2010, USA

C. Borean, C. Bozzi, L. Piemontese

Università di Ferrara, Dipartimento di Fisica and INFN, I-44100 Ferrara, Italy

E. Treadwell

Florida A&M University, Tallahassee, FL 32307, USA

F. Anulli,¹ R. Baldini-Ferroli, A. Calcaterra, R. de Sangro, D. Falciai, G. Finocchiaro, P. Patteri,
I. M. Peruzzi,² M. Piccolo, Y. Xie, A. Zallo

Laboratori Nazionali di Frascati dell'INFN, I-00044 Frascati, Italy

S. Bagnasco, A. Buzzo, R. Contri, G. Crosetti, M. Lo Vetere, M. Macri, M. R. Monge, S. Passaggio,
F. C. Pastore, C. Patrignani, E. Robutti, A. Santroni, S. Tosi

Università di Genova, Dipartimento di Fisica and INFN, I-16146 Genova, Italy

¹ Also with Università di Perugia, I-06100 Perugia, Italy

² Also with Università di Perugia, I-06100 Perugia, Italy

M. Morii

Harvard University, Cambridge, MA 02138, USA

R. Bartoldus, R. Hamilton, U. Mallik

University of Iowa, Iowa City, IA 52242, USA

J. Cochran, H. B. Crawley, J. Lamsa, W. T. Meyer, E. I. Rosenberg, J. Yi

Iowa State University, Ames, IA 50011-3160, USA

G. Grosdidier, A. Höcker, H. M. Lacker, S. Laplace, F. Le Diberder, V. Lepeltier, A. M. Lutz,
S. Plaszczynski, M. H. Schune, S. Trincaz-Duvoud, G. Wormser

Laboratoire de l'Accélérateur Linéaire, F-91898 Orsay, France

R. M. Bionta, V. Brigljević , D. J. Lange, M. Mugge, K. van Bibber, D. M. Wright

Lawrence Livermore National Laboratory, Livermore, CA 94550, USA

A. J. Bevan, J. R. Fry, E. Gabathuler, R. Gamet, M. George, M. Kay, D. J. Payne, R. J. Sloane,
C. Touramanis

University of Liverpool, Liverpool L69 3BX, United Kingdom

M. L. Aspinwall, D. A. Bowerman, P. D. Dauncey, U. Egede, I. Eschrich, G. W. Morton, J. A. Nash,
P. Sanders, D. Smith

University of London, Imperial College, London, SW7 2BW, United Kingdom

J. J. Back, G. Bellodi, P. Dixon, P. F. Harrison, R. J. L. Potter, H. W. Shorthouse, P. Strother, P. B. Vidal
Queen Mary, University of London, E1 4NS, United Kingdom

G. Cowan, S. George, M. G. Green, A. Kurup, C. E. Marker, T. R. McMahon, S. Ricciardi, F. Salvatore,
G. Vaitsas

*University of London, Royal Holloway and Bedford New College, Egham, Surrey TW20 0EX, United
Kingdom*

D. Brown, C. L. Davis

University of Louisville, Louisville, KY 40292, USA

J. Allison, R. J. Barlow, J. T. Boyd, A. C. Forti, F. Jackson, G. D. Lafferty, N. Savvas, J. H. Weatherall,
J. C. Williams

University of Manchester, Manchester M13 9PL, United Kingdom

A. Farbin, A. Jawahery, V. Lillard, J. Olsen, D. A. Roberts, J. R. Schieck

University of Maryland, College Park, MD 20742, USA

G. Blaylock, C. Dallapiccola, K. T. Flood, S. S. Hertzbach, R. Kofler, V. B. Koptchev, T. B. Moore,
H. Staengle, S. Willocq

University of Massachusetts, Amherst, MA 01003, USA

B. Brau, R. Cowan, G. Sciolla, F. Taylor, R. K. Yamamoto

Massachusetts Institute of Technology, Laboratory for Nuclear Science, Cambridge, MA 02139, USA

M. Milek, P. M. Patel

McGill University, Montréal, QC, Canada H3A 2T8

F. Palombo, C. Vite

Università di Milano, Dipartimento di Fisica and INFN, I-20133 Milano, Italy

J. M. Bauer, L. Cremaldi, V. Eschenburg, R. Kroeger, J. Reidy, D. A. Sanders, D. J. Summers

University of Mississippi, University, MS 38677, USA

C. Hast, J. Y. Nief, P. Taras

Université de Montréal, Laboratoire René J. A. Lévesque, Montréal, QC, Canada H3C 3J7

H. Nicholson

Mount Holyoke College, South Hadley, MA 01075, USA

C. Cartaro, N. Cavallo,³ G. De Nardo, F. Fabozzi, C. Gatto, L. Lista, P. Paolucci, D. Piccolo, C. Sciacca

Università di Napoli Federico II, Dipartimento di Scienze Fisiche and INFN, I-80126, Napoli, Italy

J. M. LoSecco

University of Notre Dame, Notre Dame, IN 46556, USA

J. R. G. Alsmiller, T. A. Gabriel

Oak Ridge National Laboratory, Oak Ridge, TN 37831, USA

J. Brau, R. Frey, E. Grauges , M. Iwasaki, C. T. Potter, N. B. Sinev, D. Strom

University of Oregon, Eugene, OR 97403, USA

F. Colecchia, F. Dal Corso, A. Dorigo, F. Galeazzi, M. Margoni, M. Morandin, M. Posocco, M. Rotondo,
F. Simonetto, R. Stroili, E. Torassa, C. Voci

Università di Padova, Dipartimento di Fisica and INFN, I-35131 Padova, Italy

M. Benayoun, H. Briand, J. Chauveau, P. David, Ch. de la Vaissière, L. Del Buono, O. Hamon,
Ph. Leruste, J. Ocariz, M. Pivk, L. Roos, J. Stark

Universités Paris VI et VII, Lab de Physique Nucléaire H. E., F-75252 Paris, France

P. F. Manfredi, V. Re, V. Speziali

Università di Pavia, Dipartimento di Elettronica and INFN, I-27100 Pavia, Italy

E. D. Frank, L. Gladney, Q. H. Guo, J. Panetta

University of Pennsylvania, Philadelphia, PA 19104, USA

C. Angelini, G. Batignani, S. Bettarini, M. Bondioli, F. Bucci, E. Campagna, M. Carpinelli, F. Forti,
M. A. Giorgi, A. Lusiani, G. Marchiori, F. Martinez-Vidal, M. Morganti, N. Neri, E. Paoloni, M. Rama,
G. Rizzo, F. Sandrelli, G. Simi, G. Triggiani, J. Walsh

Università di Pisa, Scuola Normale Superiore and INFN, I-56010 Pisa, Italy

M. Haire, D. Judd, K. Paick, L. Turnbull, D. E. Wagoner

Prairie View A&M University, Prairie View, TX 77446, USA

J. Albert, P. Elmer, C. Lu, V. Miftakov, S. F. Schaffner, A. J. S. Smith, A. Tumanov, E. W. Varnes

Princeton University, Princeton, NJ 08544, USA

³ Also with Università della Basilicata, I-85100 Potenza, Italy

F. Bellini, G. Cavoto, D. del Re, R. Faccini,⁴ F. Ferrarotto, F. Ferroni, M. A. Mazzoni, S. Morganti,
G. Piredda, M. Serra, C. Voena

Università di Roma La Sapienza, Dipartimento di Fisica and INFN, I-00185 Roma, Italy

S. Christ, R. Waldi

Universität Rostock, D-18051 Rostock, Germany

T. Adye, N. De Groot, B. Franek, N. I. Geddes, G. P. Gopal, S. M. Xella

Rutherford Appleton Laboratory, Chilton, Didcot, Oxon, OX11 0QX, United Kingdom

R. Aleksan, S. Emery, A. Gaidot, S. F. Ganzhur, P.-F. Giraud, G. Hamel de Monchenault, W. Kozanecki,
M. Langer, G. W. London, B. Mayer, B. Serfass, G. Vasseur, Ch. Yèche, M. Zito

DAPNIA, Commissariat à l'Energie Atomique/Saclay, F-91191 Gif-sur-Yvette, France

M. V. Purohit, A. W. Weidemann, F. X. Yumiceva

University of South Carolina, Columbia, SC 29208, USA

I. Adam, D. Aston, N. Berger, A. M. Boyarski, G. Calderini, M. R. Convery, D. P. Coupal, D. Dong,
J. Dorfan, W. Dunwoodie, R. C. Field, T. Glanzman, S. J. Gowdy, T. Haas, T. Hadig, V. Halyo, T. Himel,
T. Hryna'ova, M. E. Huffer, W. R. Innes, C. P. Jessop, M. H. Kelsey, P. Kim, M. L. Kocian,
U. Langenegger, D. W. G. S. Leith, S. Luitz, V. Luth, H. L. Lynch, H. Marsiske, S. Menke, R. Messner,
D. R. Muller, C. P. O'Grady, V. E. Ozcan, A. Perazzo, M. Perl, S. Petrak, H. Quinn, B. N. Ratcliff,
S. H. Robertson, A. Roodman, A. A. Salnikov, T. Schietinger, R. H. Schindler, J. Schwiening, A. Snyder,
A. Soha, S. M. Spanier, J. Stelzer, D. Su, M. K. Sullivan, H. A. Tanaka, J. Va'vra, S. R. Wagner,
M. Weaver, A. J. R. Weinstein, W. J. Wisniewski, D. H. Wright, C. C. Young

Stanford Linear Accelerator Center, Stanford, CA 94309, USA

P. R. Burchat, C. H. Cheng, T. I. Meyer, C. Roat

Stanford University, Stanford, CA 94305-4060, USA

R. Henderson

TRIUMF, Vancouver, BC, Canada V6T 2A3

W. Bugg, H. Cohn

University of Tennessee, Knoxville, TN 37996, USA

J. M. Izen, I. Kitayama, X. C. Lou

University of Texas at Dallas, Richardson, TX 75083, USA

F. Bianchi, M. Bona, D. Gamba

Università di Torino, Dipartimento di Fisica Sperimentale and INFN, I-10125 Torino, Italy

L. Bosisio, G. Della Ricca, S. Dittongo, L. Lanceri, P. Poropat, L. Vitale, G. Vuagnin

Università di Trieste, Dipartimento di Fisica and INFN, I-34127 Trieste, Italy

R. S. Panvini

Vanderbilt University, Nashville, TN 37235, USA

⁴ Also with University of California at San Diego, La Jolla, CA 92093, USA

C. M. Brown, P. D. Jackson, R. Kowalewski, J. M. Roney
University of Victoria, Victoria, BC, Canada V8W 3P6

H. R. Band, S. Dasu, M. Datta, A. M. Eichenbaum, H. Hu, J. R. Johnson, R. Liu, F. Di Lodovico, Y. Pan,
R. Prepost, I. J. Scott, S. J. Sekula, J. H. von Wimmersperg-Toeller, S. L. Wu, Z. Yu
University of Wisconsin, Madison, WI 53706, USA

T. M. B. Kordich, H. Neal
Yale University, New Haven, CT 06511, USA

1 Introduction

The Cabibbo-favored transition $b \rightarrow c\bar{c}s$ is well established by observation [1] of B decays to a charmonium state and a kaon, such as $B \rightarrow J/\psi K$ and $J/\psi K^*$. Recent observations of the decays $B \rightarrow J/\psi\pi$ [1] and $J/\psi\rho$ [2] are evidence for the Cabibbo-suppressed transition $b \rightarrow c\bar{c}d$. The quark diagrams for these color-suppressed decays are shown in Figures 1 (a) and (b). We search for B meson decays into other final states with charmonium. Since $B \rightarrow J/\psi\pi$ is observed, the Cabibbo suppressed modes $J/\psi\eta$ and $J/\psi\eta'$ may exist at a comparable level. A further test is to search for quark combinations such as $b\bar{q} \rightarrow c\bar{c}s\bar{s}s\bar{q}$, where the $s\bar{s}$ quark pairs are produced from sea quarks or are connected via external gluons as shown in Figures 2 (a) and (b). This would be exemplified in modes such as $B \rightarrow J/\psi\phi K$. The mode $J/\psi\phi$ is a pure rescattering process, the measurement of which can help to resolve the discrete ambiguity in the $\cos(2\beta)$ measurement with $B \rightarrow J/\psi K^*$ [3]. In this paper we report a search for B decays into $J/\psi\phi$, $J/\psi\eta$, $J/\psi\eta'$, $J/\psi\phi K^+$, and $J/\psi\phi K_S^0$ and present their branching fractions or upper limits.

Using a factorization approximation with heavy quarks, A. Deandrea *et al.* [4] have predicted the branching fraction of $B \rightarrow J/\psi\eta$ to be a factor of 3.7 smaller than $B^0 \rightarrow J/\psi\pi^0$, corresponding to $\mathcal{B}(B^0 \rightarrow J/\psi\eta) = 0.54 \times 10^{-5}$ [5]. The L3 Collaboration [6] searched for this mode, found no events and set an upper limit, $\mathcal{B}(B^0 \rightarrow J/\psi\eta) < 1.2 \times 10^{-3}$ at 90% confidence level. The mode $B \rightarrow J/\psi\phi K$ has been observed by the CLEO Collaboration [7] with 10 events in $9.6 \times 10^6 B\bar{B}$ pairs with the result $\mathcal{B}(B \rightarrow J/\psi\phi K) = (8.8^{+3.5}_{-3.0} \pm 1.3) \times 10^{-5}$. In addition to yielding $c\bar{c}$ bound states, the decay $B \rightarrow X(c\bar{c}) + K$ may provide hybrid charmonium ($c\bar{c} + glue$) [8], and the hybrid state may ultimately decay into $J/\psi\phi$ in the final state $J/\psi\phi K$. No published results exist for the modes $B \rightarrow J/\psi\phi$ and $J/\psi\eta'$.

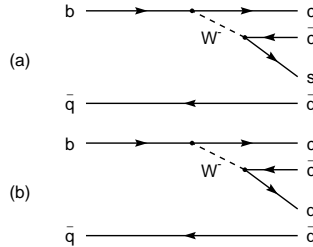


Figure 1: Quark diagrams for (a) $B \rightarrow J/\psi K$ and $J/\psi K^*$ and (b) $B \rightarrow J/\psi\pi$ and $J/\psi\rho$.

2 BABAR Detector and Dataset

The data used in this analysis were collected with the *BABAR* detector at the PEP-II asymmetric e^+e^- storage ring. The complete detector is described in detail elsewhere [9]. We briefly describe the relevant detector subsystems for the physics analysis in this paper. The *BABAR* detector contains a five-layer silicon vertex tracker (SVT) and a forty-layer drift chamber (DCH) in a 1.5-Tesla solenoidal magnetic field. These devices detect charged particles and measure their momentum and energy loss. The transverse momentum resolution is $\sigma_{p_t}/p_t = (0.13 \pm 0.01) \times p_t \% + (0.45 \pm 0.03) \%$,

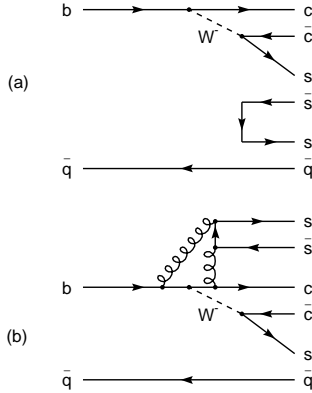


Figure 2: Quark diagrams for $B \rightarrow J/\psi\phi K$ via (a) strange sea quarks and (b) gluon coupling.

where p_t is measured in GeV/c . Photons and neutral hadrons are detected in a CsI(Tl) crystal electromagnetic calorimeter (EMC). The EMC detects photons with energies as low as 20 MeV and identifies electrons by their large energy deposit. The EMC energy resolution for photons and electrons is $\sigma(E)/E = 2.3\% / E(\text{GeV})^{1/4} + 1.9\%$. The charged particle identification (PID) combines SVT and DCH track energy loss measurements and particle velocity measurements by an internally reflecting ring-imaging Cherenkov detector (DIRC) of quartz bars circumjacent to the DCH. The slotted steel flux return is instrumented with 18-19 layers of planar resistive plate chambers (IFR). The IFR identifies penetrating muons and neutral hadrons.

The data used in these analyses were collected in two periods, October 1999 to October 2000 and February 2001 to December 2001. The data correspond to a total integrated luminosity of $\sim 51 \text{ fb}^{-1}$ taken on the $\Upsilon(4S)$ resonance and 6.3 fb^{-1} taken off-resonance at an energy 0.04 GeV below the $\Upsilon(4S)$ center of mass energy and below the threshold for $B\bar{B}$ production. This data set contains ~ 56 million $B\bar{B}$ events ($N_{B\bar{B}}$).

3 Physics Analysis

3.1 Particle Selection

This analysis begins with selection of charged particles and photons. All charged particle track candidates must have at least 12 DCH hits and $p_t > 100 \text{ MeV}/c$. The track candidates not associated with a K_s^0 decay must also extrapolate to a nominal interaction point within $\sqrt{x^2 + y^2} < 1.5 \text{ cm}$ and $|z| < 3 \text{ cm}$ where the origin is at the interaction point, the z axis is along the electron beam direction, the y axis is vertically up, and the x axis points away from the collider center. The muon, electron, and kaon candidates must have a polar angle in radians of $0.3 < \theta_\mu < 2.7$, $0.41 < \theta_e < 2.409$, and $0.45 < \theta_K < 2.5$, respectively. In addition, all charged kaon candidates used in this analysis are required to a lab momentum greater than $250 \text{ MeV}/c$. These restrictions keep the tracks in regions that are well understood by the PID systems.

Photons candidates are identified as hits in contiguous EMC crystals that are summed together to form shower clusters and have a minimum 30 MeV shower energy and satisfy certain shower shape criteria expected for electromagnetic showers. The variables that describe the shower shape include the lateral energy [10] (LAT) that determines the radial energy profile, and Zernike moment [11] (A_{42}) that measures the asymmetry of the cluster shape about its maximum. For electron showers the LAT peaks near 0.25 and A_{42} peaks near zero. All the photon candidates are required to have LAT< 0.8.

Electron candidates are required to have a good match between the expected and measured energy loss (dE/dx) and between the expected and measured DIRC Cherenkov angle (θ_C). Also the measurements of the ratio of EMC shower energy over DCH momentum (E/p), and the number of EMC crystals associated with the track candidate must be appropriate for an electron. We define very tight (VTE) and loose (LE) electron selection criteria that have efficiencies of 88% and 97%, respectively.

Muon candidates are required to have measurements of several variables that help distinguish muons from other charged particles. These measurements are: the EMC energy, the number of hit layers in the IFR, the penetration depth expressed in units of interaction length along the track's path in the IFR and EMC, the difference between the expected and measured number of interaction lengths, the average number of hits per IFR layer, the variance of the distribution of the number of hits on each IFR layer, the fraction of hit layers between the innermost and outermost layer, the chi-square match of hits in the IFR, and the chi-square match between the IFR and the extrapolated DCH track. We combine these variables to form different selection criteria applicable in different modes. The criteria are called tight (TM, efficiency 70%), loose (LM, efficiency 86%), and very loose (VLM, efficiency 92%).

Charged kaon candidates are selected based on dE/dx information from the SVT and DCH and θ_C . A likelihood function that combines all the information is constructed for the kaon, the proton and the pion hypotheses. A likelihood ratio test determines if the candidate track satisfies the loose kaon selection (LK), very tight kaon selection (VTK) or the not-a-pion selection (NP). The SVT, DCH and DIRC information and the likelihoods are used in certain selected momentum ranges. The loose and very tight selections have typical efficiencies from 70 to 90%, whereas the extremely loose selection, not-a-pion, has > 90% efficiency.

3.2 Event Selection

The estimation of the signal and the background employs two kinematic variables; the energy difference ΔE , which is the energy of the B candidate in the $\Upsilon(4S)$ frame minus the energy of the beam particle, E_{beam}^{CM} , and the energy substituted mass M_{ES} which is $\sqrt{(E_{beam}^{CM})^2 - (P_B^{CM})^2}$, where P_B^{CM} is the momentum of the B candidate in the $\Upsilon(4S)$ frame. Typically these two weakly correlated variables form a two dimensional Gaussian distribution for the B meson signal and a nearly flat two dimensional distribution for background. The resolutions in ΔE and M_{ES} can be different for different decay modes.

The intermediate state particles in this analysis are $J/\psi (ee, \mu\mu)$, $\phi (K^+ K^-)$, $\eta (\gamma\gamma, \pi^+ \pi^- \pi^0)$, $\eta' (\eta \gamma\gamma) \pi^+ \pi^-$, $\pi^0 (\gamma\gamma)$, and $K_S^0 (\pi^+ \pi^-)$. All of the intermediate state particles are selected in mass windows, which are listed in Table 1. The $J/\psi \rightarrow ee$ decay has a slightly asymmetric mass window to include the radiative J/ψ tail. Since $B^0 \rightarrow J/\psi \eta$ and $B^0 \rightarrow J/\psi \eta'$ are pseudoscalar decays into a vector and a pseudoscalar, the distribution of the helicity angle¹ of the lepton, θ_{Lepton} ,

¹ The lepton helicity angle is defined as the angle measured in the J/ψ rest frame between the direction of the

from the J/ψ is proportional to $\sin^2 \theta_{Lepton}$. Hence an additional cut of $|\cos \theta_{Lepton}| < 0.8$ is applied to reject continuum and other backgrounds. For the η candidates, a π^0 veto is applied where the candidate is rejected if either of the associated photons can be combined with another photon in the event to form a $\gamma\gamma$ mass within $20 \text{ MeV}/c^2$ of the π^0 mass. Also for the mode $B^0 \rightarrow J/\psi\eta(\gamma\gamma)$ the η candidate is rejected for asymmetric decays with $|\cos \theta_\gamma^\eta| < 0.8$, where θ_γ^η is the photon helicity angle in the η rest frame. The $\eta' \rightarrow \eta(\gamma\gamma)\pi^+\pi^-$ candidate uses the same η selections, including the π^0 veto. The mass of K_S^0 candidates is taken at the closest distance of approach between positively and negatively charged tracks.

Table 1: Mass windows used in selection of intermediate particles.

MODE	Mass Range (GeV/c^2)
$J/\psi \rightarrow e^+e^-$	$2.95 < M_{e^+e^-} < 3.14$
$J/\psi \rightarrow \mu^+\mu^-$	$3.06 < M(\mu^+\mu^-) < 3.14$
$\phi \rightarrow K^+K^-$	$1.004 < M(K^+K^-) < 1.034$
$K_S^0 \rightarrow \pi^+\pi^-$	$0.489 < M(\pi^+\pi^-) < 0.507$
$\eta \rightarrow \gamma\gamma$	$0.529 < M(\gamma\gamma) < 0.565$
$\eta \rightarrow \pi^+\pi^-\pi^0$	$0.529 < M(\pi^+\pi^-\pi^0) < 0.565$
$\eta' \rightarrow \eta\pi^+\pi^-$	$0.938 < M(\eta\pi^+\pi^-) < 0.978$
$\pi^0 \rightarrow \gamma\gamma$	$0.120 < M(\gamma\gamma) < 0.150$

An additional requirement is applied to separate and remove two-jet-like continuum events from more spherical B meson decays. The thrust direction of the B meson candidate and thrust direction of the recoiling other tracks in the event are calculated. Typically, θ_T , the angle between these two directions is uncorrelated for $B\bar{B}$ events and peaked at $\cos \theta_T = \pm 1$ for continuum events. The thrust angle requirement for the B decays is $|\cos \theta_T| < 0.8$.

The PID criteria are listed in Table 2 mode by mode. The PID requirements for some modes are slightly more stringent for background rejection.

Table 2: Particle identification requirements for each decay mode.

	$J/\psi \rightarrow e^+e^-$	$J/\psi \rightarrow \mu^+\mu^-$	$\phi \rightarrow K^+K^-$	$3^{rd} K^\pm$
$J/\psi\phi K^+$	$VTE + LE$	$VLM + LM$	$VTK + LK$	NP
$J/\psi\phi K_S^0$	$VTE + LE$	$VLM + LM$	$VTK + LK$	
$J/\psi\phi$	$VTE + VTE$	$TM + TM$	$VTK + LK$	
$J/\psi\eta$	$VTE + VTE$	$TM + TM$		
$J/\psi\eta'$	$VTE + VTE$	$TM + TM$		

negative charged lepton and the direction opposite to the parent B meson.

3.2.1 $B^0 \rightarrow J/\psi\phi$ Mode

This mode combines the J/ψ and ϕ based on the selection described in the previous section. The resulting scatter plot of ΔE versus M_{ES} is shown in Figure 3 (left top). The signal region is shown on the figure, and it is defined by $5.272 < M_{ES} < 5.288 \text{ GeV}/c^2$ and $-0.057 < \Delta E < 0.057 \text{ GeV}$. The left bottom (right) plot shows the projection onto the M_{ES} (ΔE) axis for events that satisfy the ΔE (M_{ES}) requirement for the signal region. The curve overlaid on the M_{ES} projection in this and the following figures is the sum of an ARGUS function [12] to model the combinatoric background and a Gaussian, where the Gaussian contains the background peaking in the signal region as well as the signal itself (see Section 4 for details). Statistically there is no significant signal for $B^0 \rightarrow J/\psi\phi$. An upper limit on the branching fraction is described in the next section.

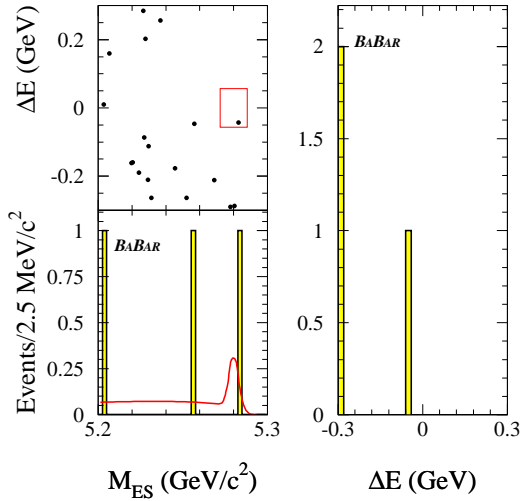


Figure 3: ΔE vs M_{ES} (left top), M_{ES} projection in ΔE signal region (left bottom), and ΔE projection in M_{ES} signal region (right) for $B^0 \rightarrow J/\psi\phi$.

3.2.2 $B \rightarrow J/\psi\phi K^+$ and $J/\psi\phi K_S^0$ Modes

In this mode we combine the J/ψ and ϕ candidates described above with a charged kaon or K_S^0 candidate. The resulting scatter plot of ΔE versus M_{ES} is shown in Figure 4 (left top) for $B^+ \rightarrow J/\psi\phi K^+$. The signal region is shown on the figure, and it is defined by $5.272 < M_{ES} < 5.288 \text{ GeV}/c^2$ and $-0.057 < \Delta E < 0.057 \text{ GeV}$. The left bottom (right) plot shows the projection onto the M_{ES} (ΔE) axis for events that satisfy the ΔE (M_{ES}) requirement for the signal region. The corresponding plots for $B^0 \rightarrow J/\psi\phi K_S^0$ are shown in Figure 5. The branching fractions are determined in the next section.

3.2.3 $B^0 \rightarrow J/\psi\eta$ Mode

For this mode, we combine a J/ψ candidate with an η candidate in the final states $\gamma\gamma$ or $\pi^+\pi^-\pi^0$. The resulting scatter plot of ΔE versus M_{ES} is shown in Figure 6 (left top) for the $\gamma\gamma$ mode and in Figure 7 (left top) for the $\pi^+\pi^-\pi^0$ mode. The left bottom plot and the right plot show the projections

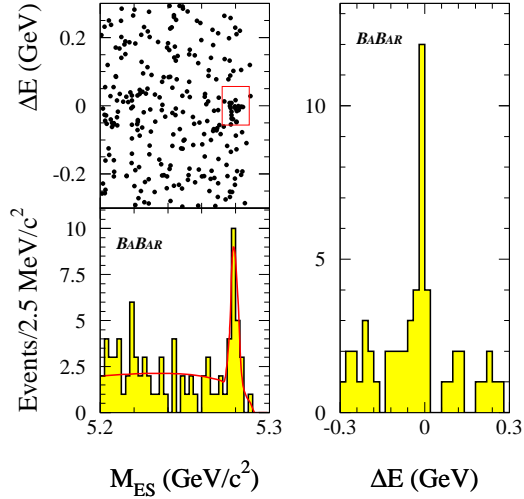


Figure 4: ΔE vs M_{ES} (left top), M_{ES} projection in ΔE signal region (left bottom), and ΔE projection in M_{ES} signal region (right) for $B^+ \rightarrow J/\psi\phi K^+$.

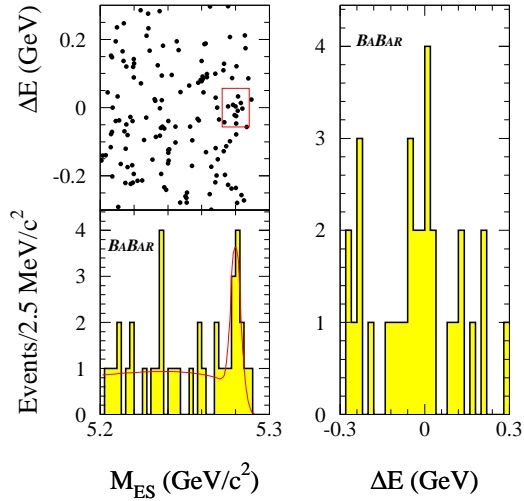


Figure 5: ΔE vs M_{ES} (left top), M_{ES} projection in ΔE signal region (left bottom), and ΔE projection in M_{ES} signal region (right) for $B^0 \rightarrow J/\psi\phi K_S^0$.

onto M_{ES} and ΔE respectively. The signal region is defined by $5.27 < M_{ES} < 5.29 \text{ GeV}/c^2$ and $-0.1 < \Delta E < 0.1 \text{ GeV}$ for the $\gamma\gamma$ mode, and $5.27 < M_{ES} < 5.29 \text{ GeV}/c^2$ and $-0.072 < \Delta E < 0.072 \text{ GeV}$ for $\pi^+\pi^-\pi^0$ mode. No statistically significant signal is observed. Upper limits on the branching fractions for these modes are described in the next section.

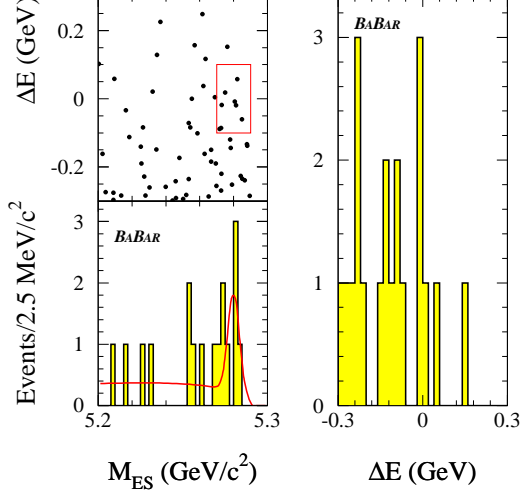


Figure 6: ΔE vs M_{ES} (left top), M_{ES} projection in ΔE signal region (left bottom), and ΔE projection in M_{ES} signal region (right) for $B^0 \rightarrow J/\psi\eta(\gamma\gamma)$.

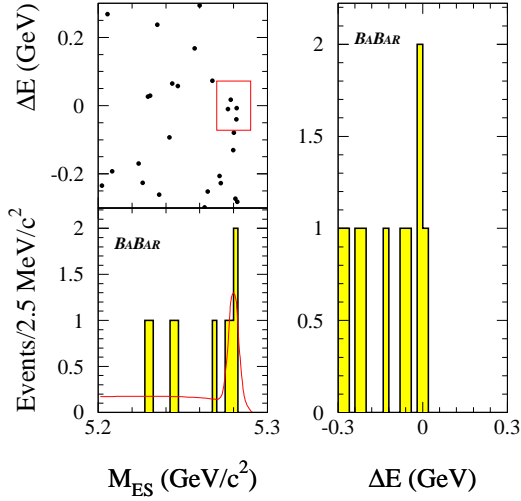


Figure 7: ΔE vs M_{ES} (left top), M_{ES} projection in ΔE signal region (left bottom), and ΔE projection in M_{ES} signal region (right) for $B^0 \rightarrow J/\psi\eta(\pi^+\pi^-\pi^0)$.

3.2.4 $B^0 \rightarrow J/\psi\eta'$ Mode

In this mode we combine J/ψ and η' candidates. The resulting scatter plot of ΔE versus M_{ES} is shown in Figure 8 (left top) for $B^0 \rightarrow J/\psi\eta'$. The signal region is defined by $5.27 < M_{ES} < 5.29 \text{ GeV}/c^2$ and $-0.1 < \Delta E < 0.1 \text{ GeV}$. The left bottom (right) plot shows the projected M_{ES} (ΔE) distribution for events that satisfy the ΔE (M_{ES}) requirement for the signal region. There is no significant evidence for $B^0 \rightarrow J/\psi\eta'$. An upper limit on the branching fraction is determined in

the next section.

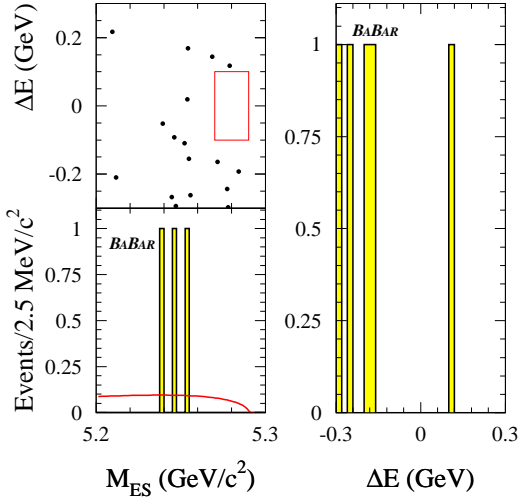


Figure 8: ΔE vs M_{ES} (left top), M_{ES} projection in ΔE signal region (left bottom), and ΔE projection in M_{ES} signal region (right) for $B^0 \rightarrow J/\psi\eta'$.

4 Efficiencies, Backgrounds and Systematic Uncertainties

The efficiencies for each mode are determined by Monte Carlo simulation where three-body phase space is assumed for the three body modes ($J/\psi\phi K^+$, $J/\psi\phi K_S^0$), two-body phase space for the vector-vector mode ($J/\psi\phi$), and helicity amplitude matrix elements for vector-pseudoscalar modes ($J/\psi\eta$, $J/\psi\eta'$). The statistical error due to the number of Monte Carlo events is included as part of the systematic error.

The background in the M_{ES} distributions can be described by an ARGUS function for the combinatoric background, plus a Gaussian function for the peaking background. The combinatoric background, denoted N_{ARGUS} , is due to continuum events, $B\bar{B}$ events with at least one J/ψ , and $B\bar{B}$ events without a J/ψ . The peaking background, denoted $N_{J/\psi-\text{Gauss}}$, comes only from $B\bar{B}$ events with a J/ψ . The shape of the ARGUS term is determined mode by mode by fitting an ARGUS function to the M_{ES} distribution from a special set of events in the data where the J/ψ is replaced by a fake J/ψ . The fake J/ψ is selected with identical selection criteria in each mode except for logically reversing the lepton identification. This provides a large sample in each mode whose M_{ES} distribution can be fitted and represents the ARGUS shape. The normalization of the combinatoric background for each mode is obtained from a fit to the M_{ES} distributions in the ΔE signal region of the on-peak data. The integral of this function in the signal region is N_{ARGUS} . This method of determining N_{ARGUS} has been checked with Monte Carlo simulation, off-peak data and ΔE and J/ψ mass sidebands from on-peak data. The peaking background $N_{J/\psi-\text{Gauss}}$ is determined from a sample of Monte Carlo $B\bar{B}$ events that is normalized to the equivalent data integrated luminosity and contains at least one decay of $J/\psi \rightarrow \text{leptons}$. The M_{ES} distribution from this sample is fit with an ARGUS function and a Gaussian in the ΔE signal region where the normalizations are allowed to vary. The number of events in the resulting

Gaussian fit is the Monte Carlo estimation of the peaking background $N_{J/\psi-Gauss}$. The sum of N_{ARGUS} plus $N_{J/\psi-Gauss}$ gives n_b , the total number of background candidates in the signal region and its error, σ_b . The combinatoric background is by far the dominant background in all modes except the $B^0 \rightarrow J/\psi\eta(\pi^+\pi^-\pi^0)$ mode, where the peaking component reaches $\sim 20\%$ of the total background.

The following sources of systematic uncertainty are considered.

- Uncertainty in the number of $B\bar{B}$ events (column labeled $\Delta N_{B\bar{B}}$ in Table 3).
- Uncertainty from secondary branching fractions (column labeled SBF in Table 3).
- Monte Carlo statistical error (column labeled MC in Table 3).
- Uncertainties in PID, tracking efficiency and photon detection efficiency (column labeled PidTrkG in Table 3).
- Variations in the event selection criteria (column labeled EvtSel in Table 3).
- Background parameterization (column labeled BkgdP in Table 3).

The secondary branching fraction uncertainty combines all errors from the Particle Data Group (PDG) [13] for each mode. The fractional uncertainty in $N_{B\bar{B}}$ is 1.6%. The uncertainty from PID, tracking efficiency and photon detection efficiency is based on the study of the control samples. The uncertainty due to event selection includes varying all event selection criteria by a reasonable amount and determining the effect on the branching fraction. The uncertainty from background parameterization is estimated by using ΔE sideband information. The largest systematic error comes from varying the event selection criteria and no single variation dominates this systematic in any mode.

The total systematic error combines all these separate errors in quadrature mode by mode. The individual systematic uncertainties are listed in Table 3.

Table 3: Systematic error summary.

Mode	$\Delta N_{B\bar{B}}$	SBF	MC	PidTrkG	EvtSel	BkgdP	Total (σ_T)
$J/\psi\phi$	1.6%	2.2%	1.6%	6.7%	11.7%	12.0%	18.3%
$J/\psi\phi K^+$	1.6%	2.2%	1.6%	8.2%	11.5%	5.9%	15.6%
$J/\psi\phi K_S^0$	1.6%	2.2%	2.1%	8.3%	14.8%	1.9%	17.5%
$J/\psi\eta(\gamma\gamma)$	1.6%	1.8%	1.6%	2.9%	14.3%	6.9%	16.4%
$J/\psi\eta(3\pi)$	1.6%	2.4%	2.2%	7.7%	13.9%	8.0%	16.5%
$J/\psi\eta'$	1.6%	3.8%	4.6%	5.7%	11.7%	7.1%	16.1%

5 Branching Fractions and Upper Limits

The branching fraction determination uses a simple subtraction of events in the signal region. The number of signal events is $n_s = n_0 - n_b$, where the term n_0 is the number of data events in the signal region, and n_b is the total background described in Section 4.

The modes $J/\psi\phi K^+$ and $J/\psi\phi K_S^0$ have significant signals: $J/\psi\phi K^+$ is 3.1 statistical standard deviations from zero, while $J/\psi\phi K_S^0$ is 2.7 statistical standard deviations from zero. The calculated branching fraction is based on the Monte Carlo efficiency, n_s , $N_{B\bar{B}}$, and the secondary branching fractions for the J/ψ , ϕ , and K_S^0 from PDG [13]. The results are summarized in Table 4 including the total summed background events in the signal region. The first error is the statistical error, and the second error is the systematic error σ_T taken from Table 3. The derived result for $B^0 \rightarrow J/\psi\phi K^0$ is also shown in Table 4.

Table 4: Branching fractions for $J/\psi\phi K^+$, $J/\psi\phi K_S^0$ and the derived result for $J/\psi\phi K^0$.

Mode	Efficiency	n_0	$n_s \pm \sigma(n_s)$	$n_b \pm \sigma_b$	Branching Fraction
$J/\psi\phi K^+$	10.6%	23	15.2 ± 4.8	7.8 ± 0.6	$(4.4 \pm 1.4(stat) \pm 0.7(syst)) \times 10^{-5}$
$J/\psi\phi K_S^0$	8.6%	13	9.7 ± 3.6	3.3 ± 0.4	$(5.1 \pm 1.9(stat) \pm 0.9(syst)) \times 10^{-5}$
$J/\psi\phi K^0$					$(10.2 \pm 3.8(stat) \pm 1.8(syst)) \times 10^{-5}$

For the modes with no signal or weak statistical evidence ($J/\psi\phi$, $J/\psi\eta$, $J/\psi\eta'$) an upper limit is set. The upper limit method uses the number of data events counted in the signal region, n_0 , n_b , and its error σ_b (described in Section 4), in the signal region and the total systematic uncertainty σ_T (%) from Table 3. Once we obtain n_0 , $n_b \pm \sigma_b$, and σ_T , then we assume these two uncertainties (σ_b , σ_T) are uncorrelated and Gaussian, the upper limit $N_{90\%}$ is obtained by folding the Poisson distribution with two normal distributions for these two uncertainties and integrating it to the 90% confidence level. We list the variables in Table 5 to obtain, $N_{90\%}$, the number of events for a 90% upper confidence limit. Then using the upper limit $N_{90\%}$, the efficiency and $N_{B\bar{B}}$, we determine the resulting upper limits on the branching fractions which are also shown in Table 5.

Table 5: 90% upper confidence limits.

Mode	Efficiency	n_0	$n_b \pm \sigma_b$	σ_T (%)	$N_{90\%}$	90% C.L. Upper Limit
$B \rightarrow J/\psi\phi$	12.1%	1	0.3 ± 0.2	18.3	3.70	$< .95 \times 10^{-5}$
$B \rightarrow J/\psi\eta (\gamma\gamma)$	15.5%	8	1.7 ± 0.4	16.4	11.8	$< 3.0 \times 10^{-5}$
$B \rightarrow J/\psi\eta (\pi^+\pi^-\pi^0)$	8.7%	4	1.5 ± 0.9	16.5	6.86	$< 5.2 \times 10^{-5}$
$B \rightarrow J/\psi\eta$ combined						$< 2.7 \times 10^{-5}$
$B \rightarrow J/\psi\eta'$	2.5%	0	0.5 ± 0.3	16.1	1.84	$< 6.4 \times 10^{-5}$

6 Conclusions

We observe evidence for $B \rightarrow J/\psi\phi K$ in two modes and determine the branching fractions $\mathcal{B}(B \rightarrow J/\psi\phi K^+) = (4.4 \pm 1.4(stat) \pm 0.7(syst)) \times 10^{-5}$ and $\mathcal{B}(B \rightarrow J/\psi\phi K_S^0) = (5.1 \pm 1.9(stat) \pm 0.9(syst)) \times 10^{-5}$. The branching fraction for $B \rightarrow J/\psi\phi K$ is consistent with CLEO results [7]. Upper limits have been determined for the modes $B \rightarrow J/\psi\phi$, $J/\psi\eta$, and $J/\psi\eta'$. However, the two $B \rightarrow J/\psi\eta$ upper limits in Table 5 would correspond to a combined branching fraction of $(1.6 \pm 0.6(stat.) \pm 0.2(syst.)) \times 10^{-5}$, which is comparable to the $B \rightarrow J/\psi\pi^0$ branching fraction.

7 Acknowledgments

We are grateful for the extraordinary contributions of our PEP-II colleagues in achieving the excellent luminosity and machine conditions that have made this work possible. The success of this project also relies critically on the expertise and dedication of the computing organizations that support *BABAR*. The collaborating institutions wish to thank SLAC for its support and the kind hospitality extended to them. This work is supported by the US Department of Energy and National Science Foundation, the Natural Sciences and Engineering Research Council (Canada), Institute of High Energy Physics (China), the Commissariat à l’Energie Atomique and Institut National de Physique Nucléaire et de Physique des Particules (France), the Bundesministerium für Bildung und Forschung (Germany), the Istituto Nazionale di Fisica Nucleare (Italy), the Research Council of Norway, the Ministry of Science and Technology of the Russian Federation, and the Particle Physics and Astronomy Research Council (United Kingdom). Individuals have received support from the A. P. Sloan Foundation, the Research Corporation, and the Alexander von Humboldt Foundation.

References

- [1] M. Alam *et al.* [CLEO collaboration], Phys. Rev. **D34**, 3279 (1986);
B. Aubert *et al.* [*BABAR* collaboration], Phys. Rev. **D65**, 32001 (2002).
- [2] M. Bishai *et al.* [CLEO Collaboration], Phys. Lett. **B369**, 186 (1996);
BABAR Collaboration, Measurement of the Branching Fraction $B^0 \rightarrow J/\psi\pi\pi$, presented to this conference.
- [3] A. Dighe, I. Dunietz, R. Fleischer, Phys. Lett. **B433**, 147 (1998);
M. Suzuki, Phys. Rev. **D64**, 117503 (2001).
- [4] A. Deandrea *et al.*, Phys. Lett. **B318**, 549 (1993).
- [5] We use $\mathcal{B}(B^0 \rightarrow J/\psi\pi^0) = (2.0 \pm 0.6 \pm 0.2) \times 10^{-5}$ from the *BABAR* Collaboration, Phys. Rev. **D65**, 32001 (2002).
- [6] M. Acciarri *et al.* [L3 Collaboration], Phys. Lett. **B391**, 481 (1997).
- [7] A. Anastassov *et al.* [CLEO Collaboration], Phys. Rev. Lett. **84**, 1393 (2000).
- [8] F. E. Close, I. Dunietz, P.R. Page, S. Veseli and H. Yamamoto, Phys. Rev. **D57**, 5653 (1998).
- [9] B. Aubert *et al.* [*BABAR* Collaboration], Nucl. Instr. and Methods **A479**, 1 (2002).
- [10] A. Drescher *et al.*, Nucl. Instr. and Methods **A237**, 464 (1985).
- [11] Ralph Sinkus and Thomas Voss, Nucl. Instr. and Methods **A391**, 360 (1997).
- [12] H. Albrecht *et al.* [ARGUS Collaboration], Z. Phys **C48**, 543 (1990).
- [13] D.E. Groom *et al.* [Particle Data Group], Eur. Phys. J. C. **15**, 1 (2000).